Cellulose (2020) 27:4691–4705
https://doi.org/10.1007/s10570-020-03112-x

ORIGINAL RESEARCH

Superhydrophobic–superoleophilic copper–graphite/styrene–butadiene–styrene based cotton filter for efficient separation of oil derivatives from aqueous mixtures

Farshad Beshkar · Masoud Salavati-Niasari · Omid Amiri

Received: 5 October 2019 / Accepted: 19 March 2020 / Published online: 27 March 2020

Abstract A superhydrophobic/superoleophilic cotton fabric composed of copper–graphite/styrene–butadiene–styrene (Cu–G/SBS) nanocomposites on the cellulose fibers has been fabricated and used as a filter for separation of gas condensates and oily solvents from aqueous mixture. First, hierarchical flower-like Cu–G nanocomposites were prepared by controlling the reduction reaction parameters such as type of reducing agent, surfactant, reaction time and weight ratio of copper to graphite. Thereafter, the coating composition of Cu–G and SBS mixtures were applied on the surface of cotton fabric by a facile dip-coating approach. Contact angle analysis of modified cotton fabric by Cu–G–SBS composites exhibited water contact angle and oil contact angle about 152° and 0°, respectively. When the superhydrophobic/superoleophilic cotton fabric was employed as a filter to separate oily solvent from water and high separation efficiency above 94% with good recyclability and stability was obtained. The result suggests that as-fabricated cotton fabric filter can be used for efficient oil/water separation in industrial applications.

F. Beshkar · M. Salavati-Niasari (✉)
Institute of Nano Science and Nano Technology, University of Kashan, P. O. Box 87317-51167, Kashan, Islamic Republic of Iran
e-mail: salavati@kashanu.ac.ir

O. Amiri
Department of Chemistry, College of Science, University of Raparin, Rania, Kurdistan Region, Iraq

Keywords Superhydrophobic · Copper–graphite nanocomposites · Cotton filter · Styrene–butadiene–styrene · Oil/water separation

Introduction

In recent years, superhydrophobic surfaces with a water contact angle greater than 150° and sliding angle less than 10° have received more attention due to their potential applications in areas of self-cleaning, oil/water separation, anti-fogging, anti-icing, antifouling, anticorrosion and energy conversion (Cao et al. 2017; Wu et al. 2019; Uzoma et al. 2019). It is generally accepted that super water-repellent surfaces are fabricated by a dual combination of micro/nanoscale surface roughness and low-surface-energy materials (Cheng et al. 2017; Razmjou et al. 2019). Moreover, design of hierarchical micro-nanostructures combined with hydrophobic modifiers can enhance surface hydrophobicity, because abundant air trapped in the interface between water and hierarchical substrate can suspend water droplet upon surface (Su et al. 2015; Beshkar et al. 2017a, b).

Graphite as a 3D network of carbon atoms arranged like a honeycomb lattice, due to its excellent electrical, mechanical, thermal, optical and hydrophobicity properties, has been extensively used in fuel cells, shields and electrodes, lithium-ion batteries, lubricants, water purification, electrical products and oil–

water separation (Jara et al. 2019; Gao et al. 2011; Bentini et al. 2019). Furthermore, it has been reported that graphite and its derivatives have some benefits for preparing superhydrophobic surfaces including inherent hydrophobicity, enhanced surface roughness and especially generating multifunctional surfaces (Hong et al. 2012; Gholami et al. 2019). Thus, some attempts have been made to fabricate graphite-based composites for improving the performance of superhydrophobicity such as octadecylamine-functionalized graphite oxide, graphite nanoplatelet/vapor-grown carbon fiber/polypropylene, expanded polystyrene foam/graphite, expanded graphite/carbon nanotube/polybenzoxazine and aluminum or copper/graphite (Lin et al. 2010; Shen et al. 2015; Sahoo et al. 2014; Wang et al. 2016; Hejazi and Nosonovsky 2012; Orooji et al. 2019a, b, c, d). Generally, metal and semiconductor nanoparticles can be loaded on graphite and its derivatives using chemical functional groups, electrostatic interactions and hydrophobic interactions (Mondal et al. 2013; Hagihghi et al. 2019; Hassandoost et al. 2019).

In the past few decades, noble metal nanostructures have attracted attention in modern nanoscience and nanotechnology owing to their unique electrical, optical, mechanical and thermal properties. In particular, metallic copper nanomaterials are promising for many future applications in electrodes, solar cells, catalysts, sensors, medical, lithium ion batteries and wear resistance fields (Bhanushali et al. 2015; Zhai et al. 2019). Lately, some researchers have successfully loaded Cu nanoparticles on graphite and its derivatives in order to expand their potential use for novel applications (Bhanushali et al. 2015; Nazeer et al. 2019). For example, Zhang et al. 2018 fabricated porous copper/graphite via a template-free strategy with excellent properties of wear and corrosion shielding. Nazeer et al. (2019) successfully synthesized copper–graphite and copper-reduced graphene oxide composites by powder metallurgy technique and investigated their anisotropic thermal conductivity and Vickers hardness. Kavaliauskas et al. (2019) prepared graphite–copper composites by plasma spray process and evaluated its microhardness, plasticity and electrical properties.

Poly(styrene–butadiene–styrene) or SBS is a triblock copolymer-based thermoplastic elastomer which is extensively used in many industrial applications due to its thermal resistance, anti-aging, abrasion resistance, anti-corrosion, durability, cost-effective, flexibility and hydrophobicity properties (Tan et al. 2016; Wang and Mao 2019; Duong et al. 2018). It has been reported that the properties of SBS polymer can be further enhanced by adding small amount of nanomaterials such as graphene, silica, carbon nanotube and copper powders (Liu et al. 2011; Vo et al. 2011; Costa et al. 2014; Harandi et al. 2017). Therefore, by combination of metal, carbon and SBS components, an interesting composite with excellent properties can be obtained.

Herein, we developed a facile and low-cost method to fabricate a superhydrophobic/superoleophilic cotton fabric filter using hierarchical flower-like Cu–G nanocomposites and SBS polymer for separation of gas condensates and other oily solvents from water. First, different morphologies of Cu–G nanostructures including sheet-like, flower-like and cactus-like were prepared by controlling the reduction reaction parameters including type of reducing agent, surfactant, reaction time and weight ratio of copper to graphite. Then, the coating composition of Cu–G and SBS mixtures were applied on the surface of cotton fabric by a simple dip-coating route. The results indicated that the modified cotton fabric filter has superhydrophobic and superoleophilic properties, which can separate gas condensates from water by a separation efficiency of 97%. The advantages of scalable production, reusability, high efficiency, cost-effective, time saving and flexibility for Cu–G–SBS/cotton fabric filter make it to be a potential candidate for oil/water separation in industrial-scale applications.

Experimental

Material and characterization

In this study, all the chemicals used for the fabrication of Cu–G/SBS nanocomposites containing $CuCl_2{\cdot}2H_2O$, ethylene diamine, graphite (G), hydrazine hydrate (80%), sodium borohydride ($NaBH_4$), styrene–butadiene–styrene (SBS), *n*-hexane, cetyl trimethyl ammonium bromide (CTAB), sodium dodecyl sulphate (SDS), poly(vinyl pyrrolidone)-25000 (PVP-25000), acetone, chloroform, petroleum ether and ethanol were purchased from Merck Company and used without purification. Scanning electron microscopy (SEM) images were obtained by Zeiss EVO scanning

Table 1 Details of the synthesis of Cu–G nanocomposites and their WCA results

Sample no.	Reducing agent	Surfactant	Reaction time (h)	Copper to graphite (wt%)	Water contact angle (°)	Figure of FESEM images
1	Hydrazine	CTAB	5	5	135	4a
2	Hydrazine	CTAB	5	10	152	4b
3	Hydrazine	CTAB	5	20	150	4c
4	Hydrazine	CTAB	1	10	137	5a
5	Hydrazine	CTAB	3	10	144	5b
6	Hydrazine	PVP25000	5	10	130	6a
7	Hydrazine	SDS	5	10	125	6b
8	Hydrazine	–	5	10	–	6c
9	$NaBH_4$	CTAB	5	10	132	7

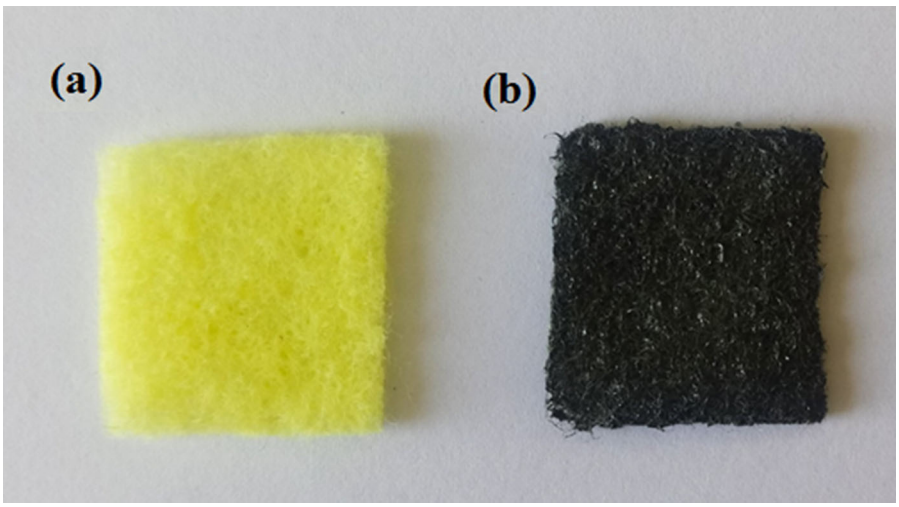

Fig. 1 Color change in cotton fabric: **a** un-coated and **b** coated cotton fabric by Cu–G nanocomposite and SBS polymer

electron microscope. X-ray diffraction (XRD) patterns were recorded by a Philips-X'PertPro, X-ray diffractometer using Ni-filtered Cu Kα radiation at scan range of $10 < 2\theta < 80$. Water contact angles (WCAs) were measured using a contact-angle meter (Veho USB microscope 400×, china) equipped with a CCD camera at room temperature. Energy dispersive X-ray spectroscopy (EDS) analysis was studied by Mira3 Tescan FE-SEM. Fourier transform infrared (FT-IR) spectra were recorded on Magna-IR, spectrometer 550 Nicolet in KBr pellets of finely cut and ground fabrics in the range of 400–4000 cm^{-1}.

Synthesis of Cu–graphite nanocomposites

Copper–graphite composites were prepared by a facile and simple chemical reduction approach. First, 50 mg of graphite powder was added to 20 mL of distilled water and 5 mL of 0.2 M CTAB aqueous solution was poured into the mixture and then, was dispersed by 30 min of sonication. On the other hand, $[Cu(en)_2(H_2O)_2]Cl_2$ complex was synthesized according to our previously reported method (Beshkar et al. 2017a, b). An aqueous mixture of 5 mL of 0.016 M $[Cu(en)_2(H_2O)_2]Cl_2$ solution and 5 mL of 0.1 M CTAB solution was prepared. Next, the copper solution was added to the graphite solution under stirring condition. After 1 h of stirring at 70 °C, 3.5 mL of hydrazine as a

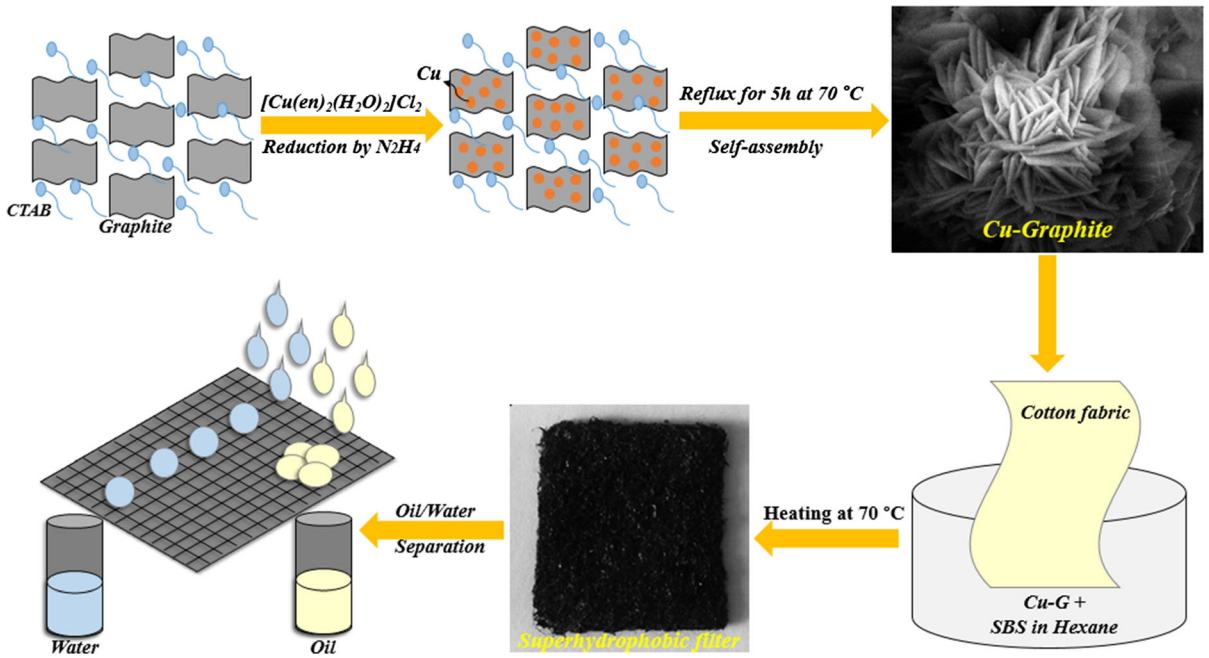

Scheme 1 Schematic design for the fabrication of superhydrophobic cotton fabric and its oil/water separation

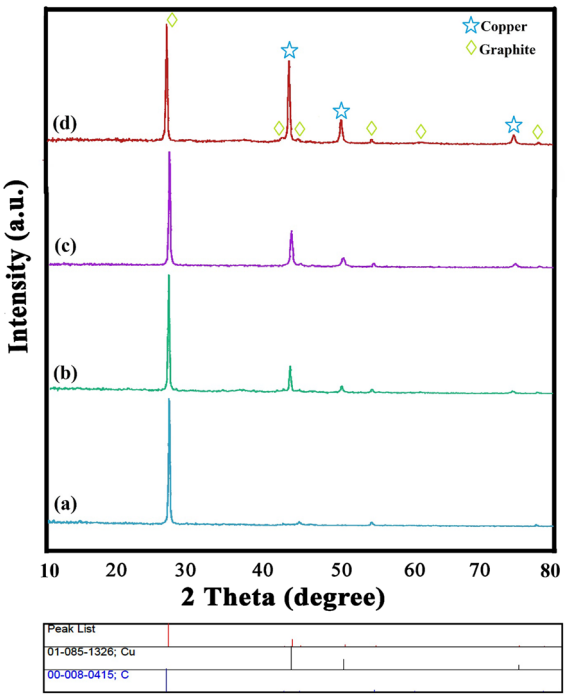

Fig. 2 XRD patterns of **a** pure graphite, **b** 5 wt% Cu–G (sample 1), **c** 10 wt% Cu–G (sample 2) and **d** 20 wt% Cu–G (sample 3)

reducing agent was added to the obtained mixture. This reaction was allowed to continue for 5 h under reflux condition for the growth of copper nanostructures on the graphite surfaces. Finally, black precipitate Cu–G nanocomposite was filtered and washed with distilled water, ethanol and dried under vacuum. In addition, the effect of the type of reducing agent, surfactant, reaction time and weight ratio of copper/graphite were studied and the obtained results illustrated in Table 1.

Preparation of superhydrophobic Cu–G–SBS/cotton fabric

First, a piece of commercial cotton fabric was cleaned with acetone, ethanol and distilled water and then, dried in an oven at 70 °C. On the other hand, Cu–G–SBS nanocomposites were prepared by mixing various amounts of Cu–G nanostructures in SBS matrix (1, 5 and 10 wt%), where n-hexane was used as an organic solvent for SBS. Each Cu–G–SBS mixture was sonicated separately before forming their respective polymer nanocomposites. For the preparation of the Cu–G–SBS/cotton fabric, the cleaned cotton fabric

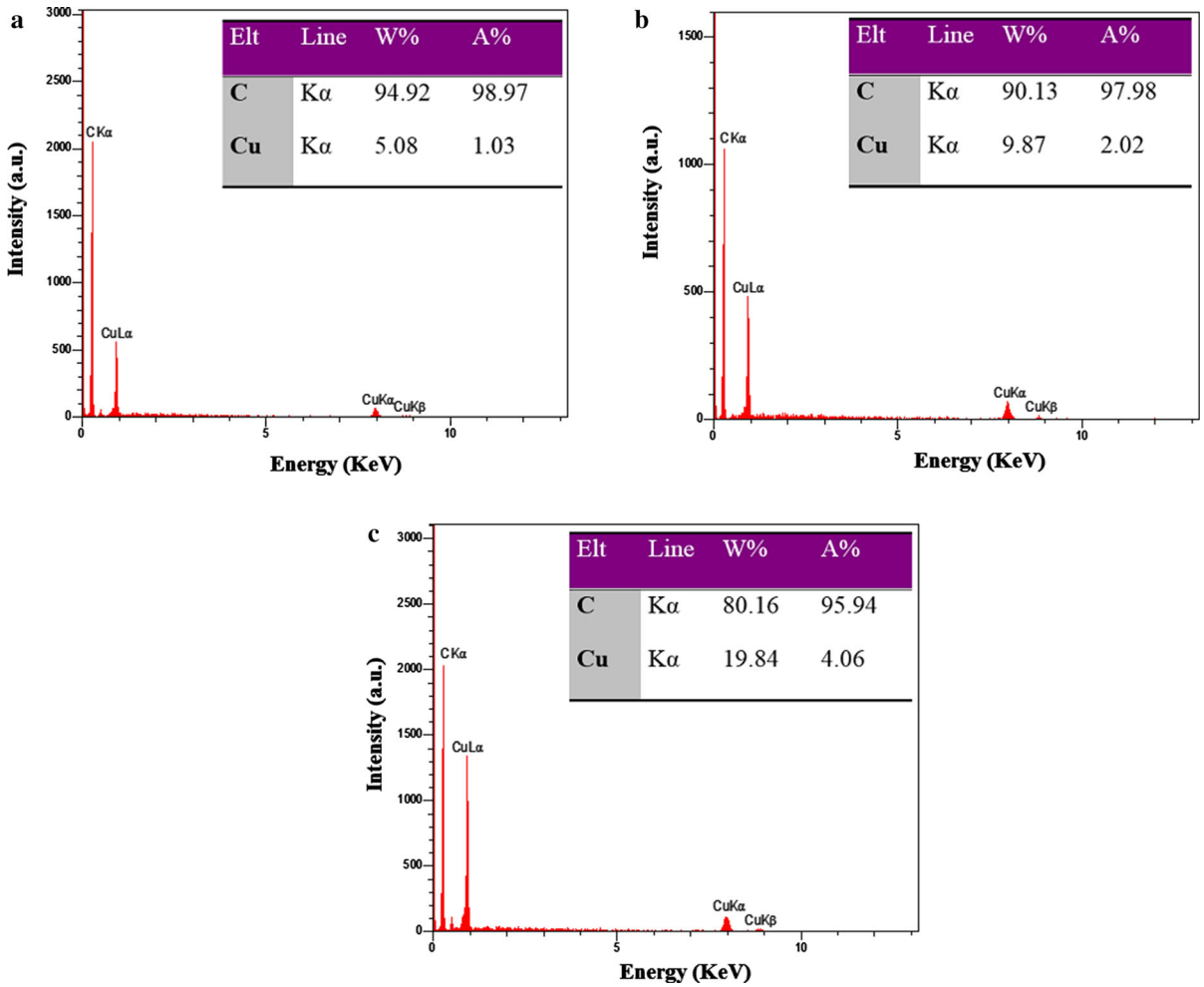

Fig. 3 EDS spectra of **a** 5 wt% Cu–G (sample 1), **b** 10 wt% Cu–G (sample 2) and **c** 20 wt% Cu–G (sample 3)

was immersed in homogeneous Cu–G–SBS dispersion and subsequently the nanocomposite was coated on the cotton fabric surfaces by vaporization of n-hexane at 70 °C and superhydrophobic cotton fabric was obtained. Figure 1 illustrates un-coated cotton fabric (a) and as-prepared superhydrophobic cotton fabric (b). Also, Scheme 1 illustrates the schematic design of the fabrication of superhydrophobic cotton fabric modified by Cu–G and SBS composite and its performance for gas condensates/water separation.

Oil/water separation of superhydrophobic cotton filter

Oil/water separation of the as-prepared superhydrophobic cotton filter was examined by separation of various oils containing gas condensates, petroleum ether, hexane and chloroform from their aqueous mixtures. In a typical experiment, 40 mL of gas condensates and water with volume ratio of 1:1 was employed. For better viewing, the water was colored by methylene blue. The superhydrophobic filter was used as a membrane filter, which was put at the bottom of syringe. The gas condensates/water mixture was dropped onto the embedded filter for the evaluation of separation performance. The gas condensates passed through the filter and fell into the flask, while water remained into the syringe. The separation efficiency (SE) of as-prepared superhydrophobic filter was estimated using the following equation:

$$SE = \frac{W_\alpha}{W_\beta} \times 100\ (\%) \quad (1)$$

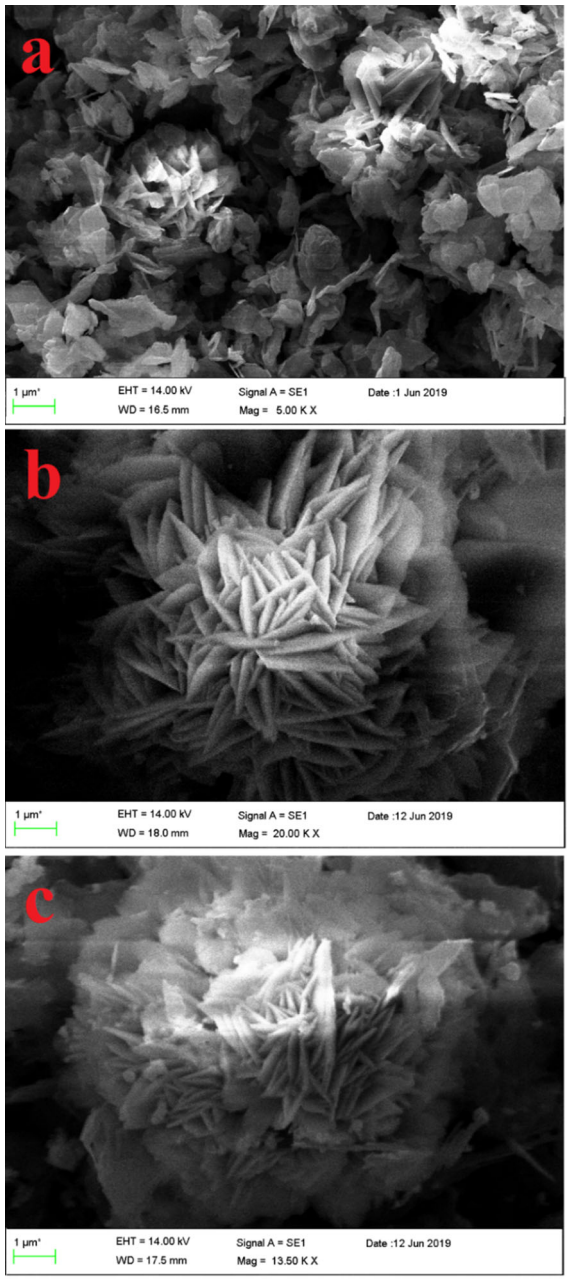

Fig. 4 SEM images for the effects of different weight percentages **a** 5 wt% Cu–G (sample 1), **b** 10 wt% Cu–G (sample 2) and **c** 20 wt% Cu–G (sample 3)

where W_β is the weight of gas condensates before separation, and W_α is the permeate weight of gas condensates after filtration.

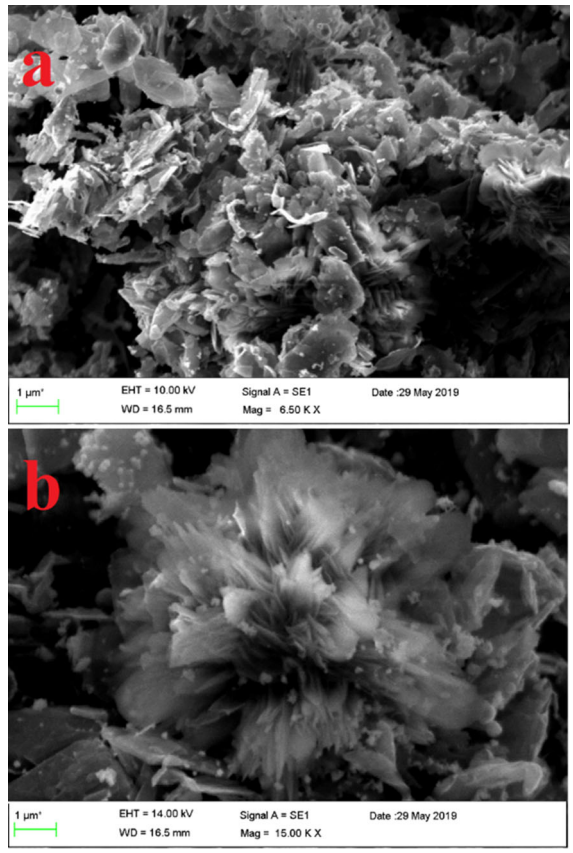

Fig. 5 SEM images for the effects of different reaction times **a** 1 h (sample 4) and **b** 3 h (sample 5)

Result and discussion

XRD and EDS characterizations

X-ray diffraction (XRD) analysis was used to characterize the as-prepared copper–graphite samples. Figures 2a–d, demonstrate XRD patterns of samples 1–3 and un-doped graphite powder. As seen in Fig. 2a, XRD pattern of pure graphite powder completely matched with the standard reference card of graphite (JCPDS No. 00-008-0415) with hexagonal crystal system. In this pattern, the main diffraction peak at 26.42° is assigned to (002) lattice planes of graphite with 0.337 nm interlayer distance. After doping 5 wt% of copper particles in graphite (sample 1), the composite powder exhibits three characteristic peaks corresponding to Cu (JCPDS No. 01-085-1326) with cubic crystal system suggesting that only zero-valent copper nanoparticles have been well deposited on the graphite surfaces (Fig. 2b). By increasing the amount

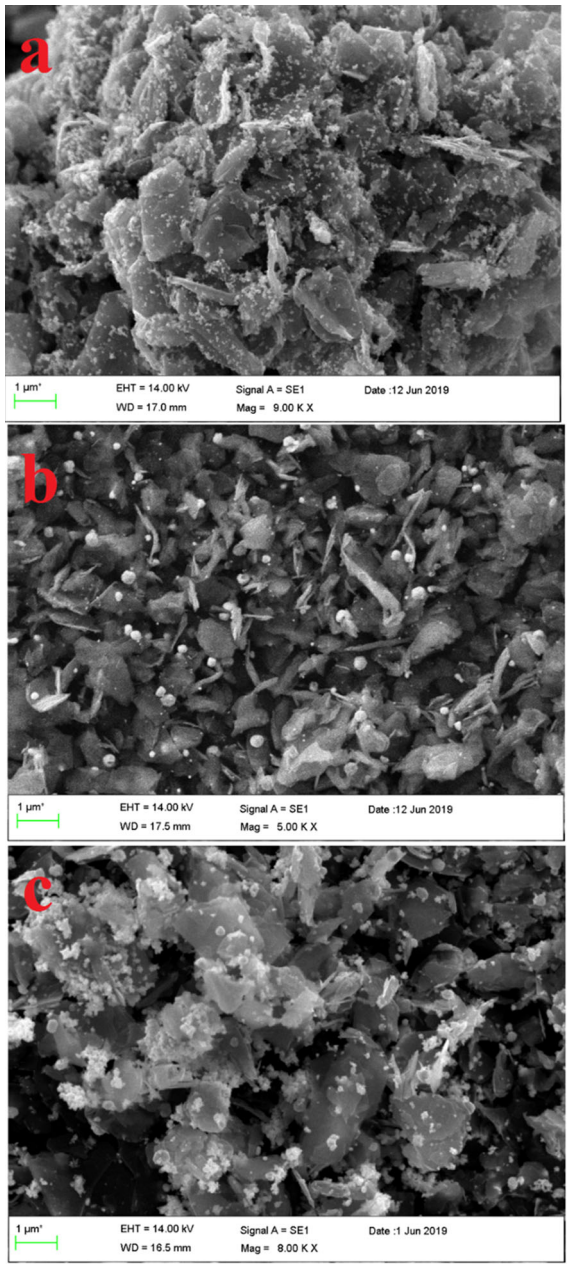

Fig. 6 SEM images for the effects of different surfactants **a** PVP25000 (sample 6), **b** SDS (sample 7) and **c** without surfactant (sample 8)

of copper in composite to 10 wt% (sample 2), the intensity of the three main peaks of Cu structure has been increased (Fig. 2c). Eventually, by raising the weight percentage of copper up to 20 (sample 3), sharp diffraction peaks of Cu with high crystalline phase were obtained (Fig. 2d). In all patterns, no

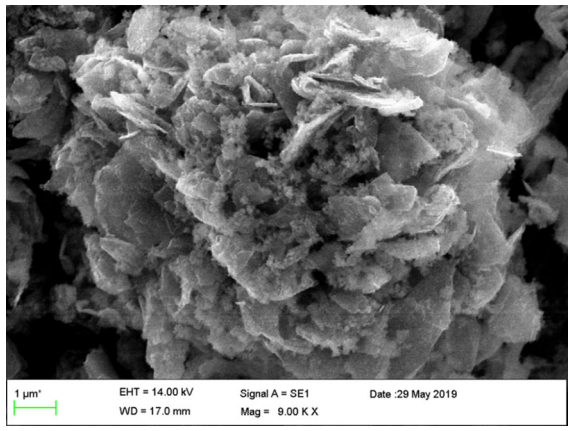

Fig. 7 SEM image for the effect of $NaBH_4$ as reducing agent on final morphology of Cu–G nanocomposite (sample 9)

characteristic peaks of any other phases of copper and graphite have been observed, which indicates high purity of products.

In addition, the elemental composition analysis of as-prepared copper–graphite nanocomposites (samples 1–3) was further confirmed by EDS analysis. As shown in Fig. 3a–c, only Cu and C elements were observed in the spectra. The quantification of Cu and C confirmed that the weight percentages of copper in graphite were about 5.08, 9.87 and 19.84 for samples 1–3, respectively (see insets), which closely agrees with the composition of Cu–G nanocomposites.

Morphology of Cu–G nanocomposites and Cu–G-coated cotton fabric

Three-dimensional flower-like copper–graphite nanocomposites were prepared by a modified chemical reduction method. In order to study the effect of reaction parameters on the morphology of Cu–G nanocomposites, the influence of reducing agent, surfactant, reaction time and weight ratio of copper to graphite was investigated. Concentration of copper precursor is an important parameter on the morphology of final products. In this case, three weight ratios of copper to graphite (5, 10 and 20 wt%) were examined by fixing the hydrazine as reducing agent, CTAB as surfactant and reaction time for 5 h. When the weight ratio was 5 wt% (sample 1), the non-assembled sheet-like Cu–G nanostructures were achieved (Fig. 4a). By increasing the weight ratio to 10 wt% (sample 2), uniform self-assembled flower-

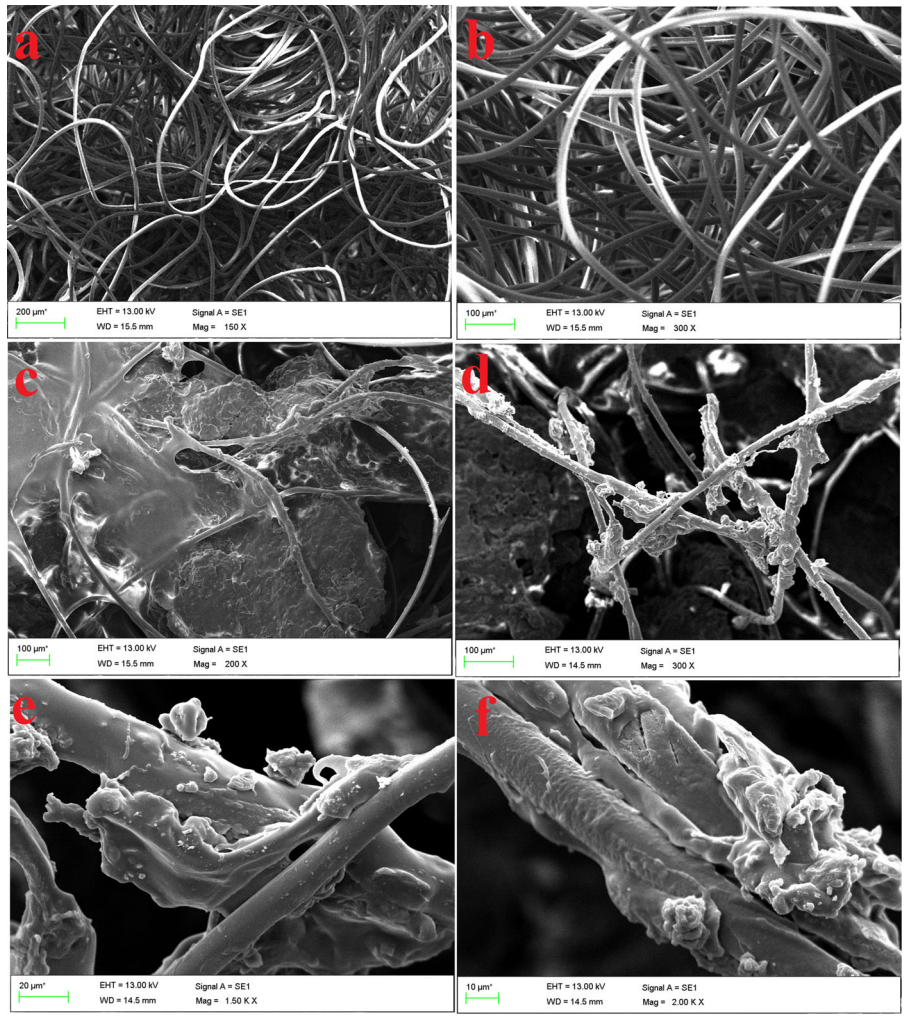

Fig. 8 SEM images of **a**, **b** pristine cotton fabric and **c–f** modified cotton fabric in the presence of Cu–G/SBS nanocomposites

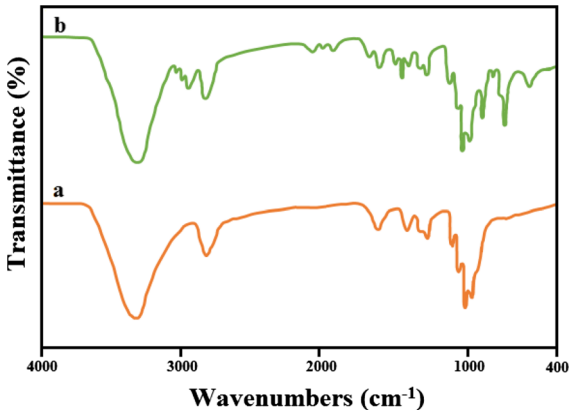

Fig. 9 FT-IR spectra of **a** pristine cotton fabric and **b** modified cotton fabric in the presence of Cu–G/SBS nanocomposites

like Cu–G nanocomposites were obtained (Fig. 4b), while the weight ratio of 20 wt% (sample 3) led to further growth of Cu–G sheets and large flower-like aggregates were generated (Fig. 4c).

Moreover, the effect of reaction time on the growth and self-assembly processes of Cu–G nanocomposites was studied. For this purpose, three different times (1, 3 and 5 h) were chosen at a constant weight ratio of Cu–G composite (10 wt%). As seen in Fig. 5a, the reaction time of 1 h was not enough for the growth and assembling of flower-like nanostructures. In this time, the agglomerated sheets of Cu–G nanocomposites were formed (sample 4). By prolonging the reaction time to 3 h (sample 5), delicate hierarchical flower-like nanostructures along with a small number of

copper nanoparticles were formed (Fig. 5b). It seems that when reaction time was further extended to 5 h (sample 2), primary copper cores had enough time for oriented growth on the graphite sheets. Thus, more copper particles were filled in free spaces between self-assembled graphite sheets, and finally uniform flower-like Cu–G nanocomposites were fabricated (Fig. 4b).

Figures 6a, b demonstrate SEM images of Cu–G composites prepared in the presence of different surfactants (SDS and PVP25000) at a constant weight ratio of Cu–G composite (10 wt%) and reaction time of 5 h. It can be seen that sheet-like nanostructures along with a large number of copper nanoparticles were prepared in the presence of PVP25000 (sample 6) and SDS (sample 7). Moreover, reduction of copper ions on the graphite sheets was performed in the absence of any surfactants (sample 8). As shown in Fig. 6c, the agglomerated sheets with copper microparticles were formed.

In addition, the effect of reducing agent on the final shape of Cu–G nanocomposites was studied. As can be

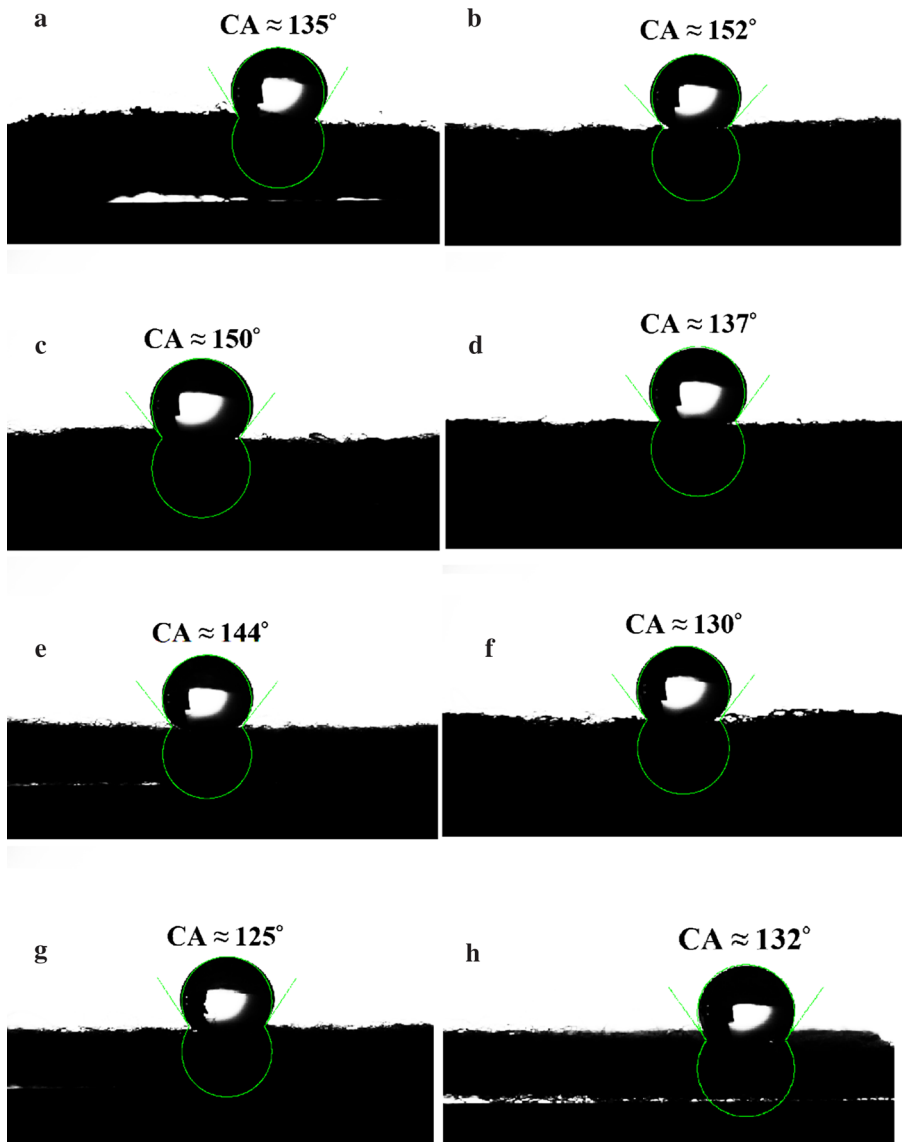

Fig. 10 **a–h** Micrographs of water contact angles on the cotton fabric surface coated by samples 1–7 and 9, respectively and SBS polymer

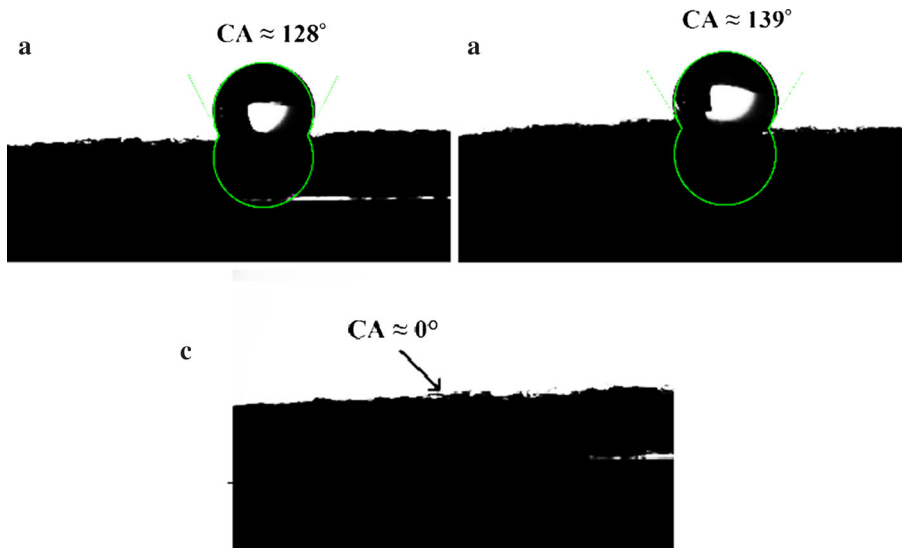

Fig. 11 Water contact angle images for different weight percentages of Cu–G to SBS **a** 1 wt% and **b** 5 wt% and **c** oil contact angle image of as-modified cotton filter

seen in Fig. 7, by using $NaBH_4$ as reducing agent, non-uniform flower-like morphology of Cu–G nanocomposite (sample 9) was obtained.

It is well known that wettability depends on the physical structure of surface. As can be seen in Fig. 8a, b, pristine cotton fabric is fabricated from an interwoven 3D network of smooth fibers. Also, pristine cotton is consists of approximately 400 thread counts per centimeter. Furthermore, SEM images of pristine cotton fabric and treated cotton fabric were demonstrated in Fig. 8a–f. It can be observed that pristine fabrics are perfectly smooth (Fig. 8a, b), while the treated fabrics covered by Cu–G/SBS nanocomposites (sample 2) exhibited high roughness (Fig. 8c–f). When the surfaces of fabrics were assembled with Cu–G/SBS layers, Cu–G micro/nanostructures were randomly dispersed on the surface and subsequently, created valleys and hills over the cotton fabric surface. From Fig. 8c–f, it is obvious that SBS polymer chains can uniformly adhere to the fabrics surface, and enhance the adhesion between Cu–G structures and fibers. Thus, by combination of surface roughness and the layer of SBS polymer, the modified cotton surface cannot be wetted by water droplets and exhibits relatively stable superhydrophobicity with water contact angle (WCA) of 152° (Fig. 10b).

FT-IR spectra of Cu–G/SBS-coated cotton fabric

For further confirmation of the modification of cotton fabric, FT-IR analysis of pristine cotton fabric and treated cotton fabric by Cu–G/SBS nanocomposites (sample no. 2) was taken and presented in Fig. 9a, b. FT-IR spectrum of pristine cotton fabric (Fig. 9a) showed some characteristic peaks at around 3421, 2903, 1437 and 1054 cm^{-1}, which are attributed to O–H stretching, C–H stretching, CH_2 symmetric bending and C–O stretching from cellulose, respectively. Also, the peak at 1637 cm^{-1} was reported for bending vibrations of –OH groups of absorbed water molecules (Xu et al. 2015; Wulandari et al. 2016). Compared to pristine cotton fabric, FT-IR spectrum of Cu–G/SBS-coated cotton fabric demonstrated some new peaks at around 1648 and 579 cm^{-1}, which are ascribed to stretching vibrations of carbon skeleton (C=C) of graphite and copper, respectively (Bharath et al. 2017; Ponraj et al. 2018). Moreover, the characteristic peaks of SBR polymer can be identified at around 3014, 2947 and 2861, 1995 and 1870, 1492 and 1463, 979 and 728 cm^{-1}, which are associated to unsaturated carbons, stretching of methyl and methylene groups, aromatic ring overtone, methyl and methylene bending vibrations, and unsaturated aromatic carbons deformations, respectively (Almazán et al. 2016).

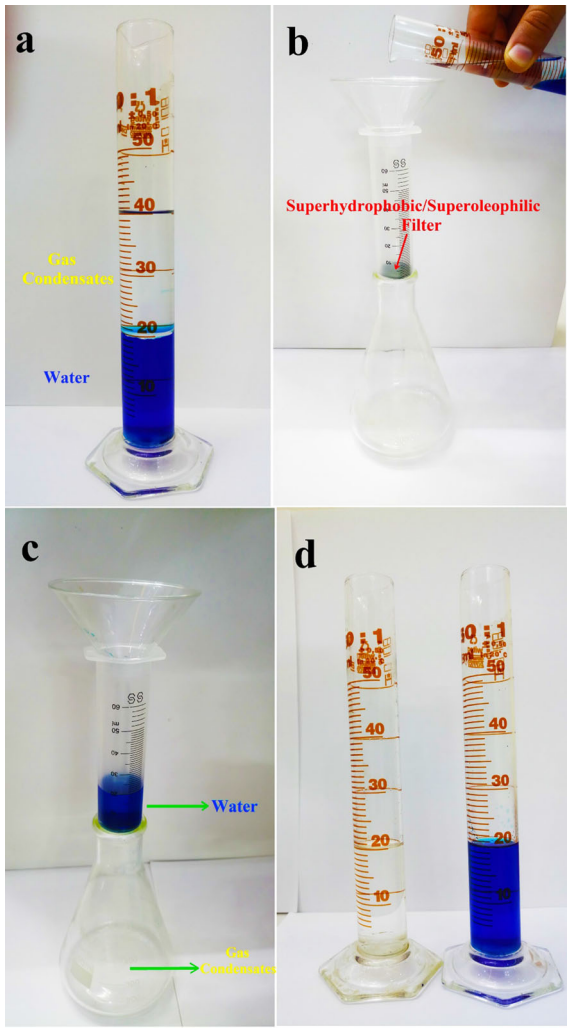

Fig. 12 Photographs of gas condensates-water separation experiment by optimized superhydrophobic/superoleophilic cotton filter. The water was colored by methylene blue

Water contact angle analysis of superhydrophobic cotton fabric

It is reported that the surface modifications by hydrophobic agents and hierarchical micro/nanostructures on a surface can influence on its wettability properties (Beshkar et al. 2017a, b). As seen in Fig. 4c, the micro/nano-protrusions created by hierarchical flower-like copper–graphite structures generated unique valleys and hills over cotton surface and subsequently, the surface became rough, which led to trap more air pockets between water droplet and surface. Hence, it is expected that as-coated cotton fabric with flower-like Cu–G nanocomposites and SBS polymer may result in a remarkable superhydrophobicity. The water contact angles (WCAs) of cotton fabrics modified by 10 wt% of different morphologies of Cu–G nanocomposites in SBS polymer were measured. The results of WCA analysis of cotton fabrics prepared with samples 1–7 and 9 are exhibited in Fig. 10a–h and Table 1. As it can be seen, all morphologies of Cu–G nanocomposites enhanced the hydrophobicity of cotton fabrics. Among them, uniform flower-like morphology (sample 2) exhibited excellent superhydrophobicity with a water contact angle of 152° (Fig. 10b). It is expected that as-synthesized hierarchical flower-like Cu–G architecture may result in a special wettability of cotton fabric.

Moreover, the weight ratio of Cu–G (sample 2) to SBS composite was examined in quantities of 1, 5 and 10 wt%. As shown in Fig. 11a, b, when the weight ratio of Cu–G to SBS was 1 wt%, WCA reached to about 128° (Fig. 11a), while by increasing the weight ratio to 5 wt%, WCA of 139° was obtained (Fig. 11b). Previously, the weight ratio of 10 wt% of Cu–G nanocomposite to SBS polymer enhanced WCA to 152° (Fig. 10b). Also, the oil contact angle of as-prepared Cu–G/SBS-coated filter was taken and illustrated the superoleophilicity with oil contact angle about 0°, which allows the oily droplets to penetrate quickly through the filter (Fig. 11c).

Oil/water separation performance of superhydrophobic/superoleophilic cotton filter

It is well known that superoleophilicity and superhydrophobicity of a filter surface are two essential factors to characterize oil/water separation. Also, the textile fabric filters are potential candidates for oil derivatives/water separation because of their softness, flexibility, selectivity and reusability (Kansara et al. 2016; Li et al. 2012). As seen in Fig. 10b, the cotton fabric exhibited superhydrophobicity with water contact angle of 152°, which caused the water droplets to remain above the filter surface, while allowing the oils to permeate easily through the cotton filter. Therefore, the gas condensates/water separation experiment was carried out by as-prepared superhydrophobic/superoleophilic cotton filter. When the gas condensates–water mixture was poured onto the filter surface, gas condensates quickly permeated through the cotton filter and rapidly dropped into the flask. On the other

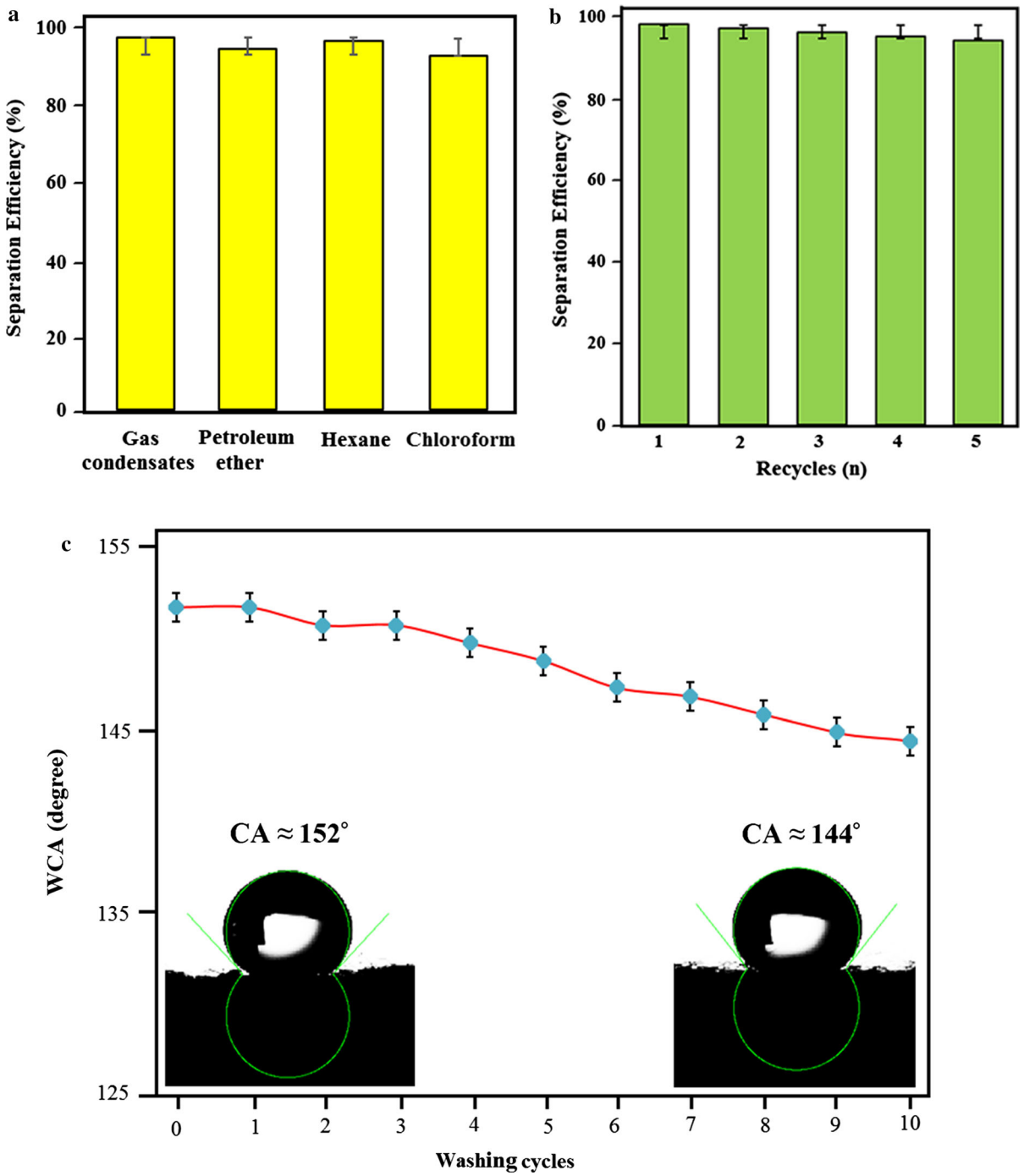

Fig. 13 **a** Separation of various oil–water mixtures, **b** recycle test of as-fabricated superhydrophobic filter for 5 times of gas condensates/water separation and **c** stability test of modified superhydrophobic cotton filter after washing and rubbing processes (error bars show the standard deviation of related measurements and insets show WCA images of primary modified cotton filter and after 10 cycles of washing and rubbing)

hand, water could not penetrate through the fabric filter and thus, remained on the filter surface in the syringe (Fig. 12a–d). After filtration, only clear and transparent gas condensates was visible which indicates high oil–water separation efficiency of as-prepared superhydrophobic cotton filter. By using Eq. (1), the separation efficiency of gas condensates from water utilizing as-prepared superhydrophobic/superoleophilic cotton filter was about 97%. The simple, time saving, high separation efficiency and gravity-driven oil/water separation of superhydrophobic cotton fabric can provide more chances for industrial applications.

Furthermore, a series of oily solvents including petroleum ether, hexane and chloroform were examined for separation ability of as-prepared superhydrophobic cotton filter. As shown in Fig. 13a, the separation efficiencies of superhydrophobic/superoleophilic cotton filter with hierarchical Cu–G/SBS coating for aqueous mixtures of petroleum ether, hexane and chloroform were about 94, 96 and 92%, respectively. In addition, the recyclability of as-coated cotton filter is a significant criterion for practical oil cleanup applications. The separation process was repeated at least five times using gas condensates as a model to study the recyclability of as-prepared filter. As demonstrated in Fig. 13b, oil separation efficiency remained stable even after 5 successive cycles. A negligible decrease in separation efficiency can be ascribed to the residual oily solvent inside the cotton filter. The above results exhibit that the superhydrophobic/superoleophilic cotton filter not only has a high separation efficiency for various oily solvents but it also has good recyclability. Moreover, the stability of the superhydrophobicity property of Cu–G/SBS-coated cotton fabric was investigated by washing and rubbing of as-modified filter for 10 cycles and the change in WCA as a function of wash cycles was recorded. As illustrated in Fig. 13c, the superhydrophobic cotton filter exhibited excellent superhydrophobic stability with WCA of about 144° after 10 cycles of washing and rubbing. This result can be attributed to good affinity between Cu–G/SBS nanocomposites and cotton fabric.

Conclusion

In summary, the superhydrophobic/superoleophilic cotton fabric filters were fabricated by flower-like copper–graphite nanocomposite and SBS polymer utilizing a green and simple dip-coating method. Various morphologies of Cu–G nanostructures were prepared by controlling the reduction reaction parameters including type of reducing agent, surfactant, reaction time and weight ratio of copper to graphite. When mixture of flower-like Cu–G nanocomposite and SBS polymer was deposited on the cotton fabric, CA analysis showed excellent superhydrophobicity and superoleophilicity properties with water contact angle and oil contact angle about 152° and 0°, respectively. Moreover, the superhydrophobic/superoleophilic cotton fabric was employed as a filter to separate gas condensates and various oil/water mixtures, which indicated that as-prepared filter had high separation efficiency and good recyclability. The result shows that the as-fabricated cotton fabric filter can be used for efficient oil/water separation in industrial-scale applications.

Acknowledgments Authors are grateful to the council of Iran National Science Foundation (97017837) and University of Kashan for supporting this work by Grant No (159271/8990).

Compliance with ethical standards

Conflict of interest There are no conflicts to declare.

References

Almazán CMDL, Chávez-Cinco MY, Páramo-García U, Mendoza-Martínez AM, Estrada-Moreno IA, Rivera-Armenta JL (2016) PANI/SBR composites as anticorrosive coatings for carbon steel I. Chemical, morphological and superficial characterization. Polym Bull 73:1595–1605

Bentini R, Pola A, Rizzi LG, Athanassiou A, Fragouli D (2019) A highly porous solvent free PVDF/expanded graphite foam for oil/water separation. Chem Eng J 372:1174–1182

Beshkar F, Khojasteh H, Salavati-Niasari M (2017a) Flower-like CuO/ZnO hybrid hierarchical nanostructures grown on copper substrate: glycothermal synthesis, characterization, hydrophobic and anticorrosion properties. Materials 10:697

Beshkar F, Zinatloo-Ajabshir S, Bagheri S, Salavati-Niasari M (2017b) Novel preparation of highly photocatalytically active copper chromite nanostructured material via a simple hydrothermal route. PLoS ONE 12(6):0158549

Bhanushali S, Ghosh P, Ganesh A, Cheng W (2015) 1D copper nanostructures: progress, challenges and opportunities. Small 11:1232–1252

Bharath G, Latha BS, Alsharaeh EH, Prakashd P, Ponpandian N (2017) Enhanced Hydroxyapatite nanorods formation on graphene oxide nanocomposite as a potential candidate for protein adsorption, pH controlled release and an effective drug delivery platform for cancer therapy. Anal Methods 9:240–252

Cao N, Yang B, Barras A, Szunerits S, Boukherroub R (2017) Polyurethane sponge functionalized with superhydrophobic nanodiamond particles for efficient oil/water separation. Chem Eng J 307:319–325

Cheng QY, An XP, Li YD, Huang CL, Zeng JB (2017) Sustainable and biodegradable superhydrophobic coating from epoxidized soybean oil and ZnO nanoparticles on cellulosic substrates for efficient oil/water separation. ACS Sustain Chem Eng 5:11440–11450

Costa P, Silva J, Anson-Casaos A, Martinez MT, Abad MJ, Viana J, Lanceros-Mendez S (2014) Effect of carbon nanotube type and functionalization on the electrical, thermal, mechanical and electromechanical properties of carbon nanotube/styrene–butadiene–styrene composites for large strain sensor applications. Compos Part B Eng 61:136–146

Duong HC, Chuai D, Woo YC, Shon HK, Nghiem LD, Sencadas V (2018) A novel electrospun, hydrophobic, and elastomeric styrene–butadiene–styrene membrane for membrane distillation applications. J Membr Sci 549:420–427

Gao W, Majumder M, Alemany LB, Narayanan TN, Ibarra MA, Pradhan BK, Ajayan PM (2011) Engineered graphite oxide materials for application in water purification. ACS Appl Mater Interfaces 36:1821–1826

Gholami P, Dinpazhoh L, Khataee A, Orooji Y (2019) Sonocatalytic activity of biochar-supported ZnO nanorods in degradation of gemifloxacin: synergy study, effect of parameters and phytotoxicity evaluation. Ultrason Sonochem 55:44–56

Hagihghi R, Razmjou A, Orooji Y, Warkiani ME, Asadnia MA (2019) Miniaturized piezoresistive flow sensor for real-time monitoring of intravenous infusion. Appl Biomater, J Biomed Mater Res B, pp 1–9

Harandi MH, Alimoradi F, Rowshan G, Faghihi M, Keivan M, Abadyan M (2017) Morphological and mechanical properties of styrene butadiene rubber/nano copper nanocomposites. Res Phys 7:338–344

Hassandoost R, Rahim Pouran S, Khataee A, Orooji Y, Joo SW (2019) Hierarchically structured ternary heterojunctions based on Ce^{3+}/Ce^{4+} modified Fe_3O_4 nanoparticles anchored onto graphene oxide sheets as magnetic visible-light-active photocatalysts for decontamination of oxytetracycline. J Hazard Mater 376:200–211

Hejazi V, Nosonovsky M (2012) Wear-resistant and oleophobic biomimetic composite materials. Green Tribol 7:149–172

Hong SJ, Li YF, Hsiao MJ, Sheng YJ, Tsao HK (2012) Anomalous wetting on a superhydrophobic graphite surface. Appl Phys Lett 100:121601

Jara AD, Betemariam A, Woldetinsae G, Kim JY (2019) Purification, application and current market trend of natural graphite: a review. Int J Min Sci Technol 29:671–689

Kansara AM, Chaudhri SG, Singh PS (2016) A facile one-step preparation method of recyclable superhydrophobic polypropylene membrane for oil–water separation. RSC Adv 6:61129–61136

Kavaliauskas Ž, Marcinauskas L, Milieška M, Valinčius V, Baltušnikas A, Žunda A (2019) Effect of copper content on the properties of graphite–copper composites formed using the plasma spray process. Surf Coat Technol 364:398–405

Li J, Shi L, Chen Y, Zhang Y, Guo Z, Su BL, Liu W (2012) Stable superhydrophobic coatings from thiol-ligand nanocrystals and their application in oil/water separation. J Mater Chem 22:9774–9781

Lin Z, Liu Y, Wong CP (2010) Facile fabrication of superhydrophobic octadecylamine-functionalized graphite oxide film. Langmuir 26:16110–16114

Liu YT, Xie XM, Ye XY (2011) High-concentration organic solutions of poly(styrene-cobutadiene-*co*-styrene)-modified graphene sheets exfoliated from graphite. Carbon 49:3529–3537

Mondal P, Sinha A, Salam N, Roy AS, Jana NR, Islam SM (2013) Enhanced catalytic performance by copper nanoparticle-graphene based composite. RSC Adv 3:5615–5623

Nazeer F, Ma Z, Gao L, Wang F, Abubaker-Khan M, Malik A (2019) Thermal and mechanical properties of copper–graphite and copper-reduced graphene oxide composites. Compos Part B Eng 163:77–85

Orooji Y, Ghasali E, Emami N, Noorisafa F, Razmjou A (2019a) ANOVA design for the optimization of TiO_2 coating on polyether sulfone membranes. Molecules 24:2924–2937

Orooji Y, Derakhshandeh MR, Ghasali E, Alizadeh M, Shahedi Asl M, Ebadzadeh T (2019b) Effects of ZrB_2 reinforcement on microstructure and mechanical properties of a spark plasma sintered mullite-CNT composite. Ceram Int 45:16015–16021

Orooji Y, Alizadeh A, Ghasali E, Derakhshandeh MR, Alizadeh M, Shahedi Asl M, Ebadzadeh T (2019c) Co-reinforcing of mullite-TiN-CNT composites with ZrB_2 and TiB_2 compounds. Ceram Int 45:20844–20854

Orooji Y, Ghasali E, Moradi M, Derakhshandeh MR, Alizadeh M, Shahedi Asl M, Ebadzadeh T (2019d) Preparation of mullite-TiB_2-CNTs hybrid composite through spark plasma sintering. Ceram Int 45:16288–16296

Ponraj NV, Azhagurajan A, Vettivel SC, Shajan XS, Nabhiraj PY (2018) Study of processing and microstructure of copper composite reinforced with graphene nanosheet by powder metallurgy technique. Powder Metall Met Ceram 56:523–534

Razmjou A, Eshaghi G, Orooji Y, Hosseini E, Habibnejad Korayem A, Mohagheghian F, Boroumand Y, Noorbakhsh A, Asadnia M, Chen V (2019) Lithium ion-selective membrane with 2D subnanometer channels. Water Res 159:313–323

Sahoo BN, Sabarish B, Balasubramanian K (2014) Controlled fabrication of non-fluoro polymer composite film with hierarchically nano structured fibers. Prog Org Coat 77:904–907

Shen L, Qiu W, Wang W, Xiao G, Guo Q (2015) Facile fabrication of superhydrophobic conductive graphite nanoplatelet/vapor-grown carbon fiber/polypropylene composite coatings. Compos Sci Technol 117:39–45

Su C, Lu Z, Zhao H, Yang H, Chen R (2015) Photoinduced switchable wettability of bismuth coating with hierarchical dendritic structure between superhydrophobicity and superhydrophilicity. Appl Surf Sci 353:735–743

Tan QC, Shanks RA, Hui D, Kong I (2016) Properties of functionalised graphene-multiwalled carbon nanotubes hybrid poly(styreneb-butadiene-b-styrene) nanocomposites. Compos Part B Eng 90:315–325

Uzoma PC, Liu F, Xu L, Zhang Z, Han EH, Ke W, Arukalam IO (2019) Superhydrophobicity, conductivity and anticorrosion of robust siloxaneacrylic coatings modified with graphene nanosheets. Prog Org Coat 127:239–251

Vo LT, Anastasiadis SH, Giannelis EP (2011) Dielectric study of poly(styrene-*co*-butadiene) composites with carbon black, silica, and nanoclay. Macromolecules 44:6162–6171

Wang F, Mao J (2019) Nacre-like graphene oxide/waterborne styrene butadiene rubber composite and its reusable anticorrosion behavior on Al-2024. Prog Org Coat 132:191–200

Wang CF, Wang WN, Yang SY, Chen LT, Tsai HY (2016) Preparation and characterization of biomimetic superhydrophobic expanded graphite/carbon nanotube/polymer composites. IEEE Xplore Digit Libr. https://doi.org/10.1109/ICEP.2016.7486916

Wu M, An R, Yadav SK, Jiang X (2019) Graphene tailored by Fe_3O_4 nanoparticles: lowadhesive and durable superhydrophobic coatings. RSC Adv 9:16235–16245

Wulandari WT, Rochliadi A, Arcana IM (2016) Nanocellulose prepared by acid hydrolysis of isolated cellulose from sugarcane gagasse. IOP Conf Ser Mater Sci Eng 107:012045

Xu LL, Guo MX, Liu S, Bian SW (2015) Graphene/cotton composite fabrics as flexible electrode materials for electrochemical capacitors. RSC Adv 5:25244–25249

Zhai W, Lu W, Chen Y, Liu X, Zhou L, Lin D (2019) Gas-atomized copper-based particles encapsulated in graphene oxide for high wear-resistant composites. Compos Part B Eng 157:131–139

Zhang G, Xie G, Wang J, Si L, Guo D, Wen S, Yang F (2018) Controlled friction behaviors of porous copper/graphite storing ionic liquid through electrical stimulation. Adv Eng Mater 20:1700866